Interfacial Nb-substitution induced anomalous enhancement of polarization and conductivity in BaTiO3...

Article *in* AIP Advances · December 2014

DOI: 10.1063/1.4905059

Yue Zheng
National University of Singapore

W. J. Chen
Sun Yat-Sen University

Interfacial Nb-substitution induced anomalous enhancement of polarization and conductivity in BaTiO3 ferroelectric tunnel junctions

H. F. Li, Yue Zheng, W. J. Chen, Biao Wang, and G. H. Zhang

Citation: AIP Advances **4**, 127148 (2014); doi: 10.1063/1.4905059
View online: http://dx.doi.org/10.1063/1.4905059
View Table of Contents: http://scitation.aip.org/content/aip/journal/adva/4/12?ver=pdfcov
Published by the AIP Publishing

AIP ADVANCES **4**, 127148 (2014)

Interfacial Nb-substitution induced anomalous enhancement of polarization and conductivity in BaTiO$_3$ ferroelectric tunnel junctions

H. F. Li,[1,2] Yue Zheng,[1,2,a] W. J. Chen,[1,2] Biao Wang,[1,b] and G. H. Zhang[1,2]
[1]*State Key Laboratory of Optoelectronic Materials and Technologies, Sun Yat-sen University, 510275, Guangzhou, China*
[2]*Micro&Nano Physics and Mechanics Research Laboratory, School of Physics and Engineering, Sun Yat-sen University, 510275, Guangzhou, China*

(Received 27 October 2014; accepted 15 December 2014; published online 22 December 2014)

Using density functional theory (DFT) method combined with non-equilibrium Green's function approach, we systematically investigated the structural, ferroelectric and electronic transport properties of Pt/BaTiO$_3$/Pt ferroelectric tunnel junctions (FTJ) with the interface atomic layers doped by charge neutral Nb$_{\mathrm{Ti}}$ substitution. It is found that interfacial Nb$_{\mathrm{Ti}}$ substitution will produce several anomalous effects such as the vanishing of ferroelectric critical thickness and the decrease of junction resistance against tunneling current. Consequently, the thickness of the ferroelectric thin film (FTF) in the FTJ can be reduced, and both the electroresistance effect and sensitivity to external bias of the FTJ are enhanced. Our calculations indicate that the enhancements of conductivity and ferroelectric distortion can coexist in FTJs, which should be important for applications of functional electronic devices based on FTJs. [http://dx.doi.org/10.1063/1.4905059]

I. INTRODUCTION

For their functional properties, ferroelectric materials play important roles in developing multifunctional electronic devices. Recent interest in ferroelectric tunnel junction (FTJ) begins to grow for reasons of both scientific curiosity and prospects of practical applications. FTJ is a capacitor structure which uses metallic material as electrodes and ferroelectric thin film as the barrier. In the nanometer scale, it is known that the ferroelectric and transport properties of ferroelectric material depend largely on its size, surface and interface which forming a boundary among it and a different material. FTJ involves both size and interface effects and exhibit a variety of polarization-related electronic transport properties such as giant electroresistance,[1–3] giant piezoresistance,[4] and nondestructive read out,[5] etc. These properties provide the possibility of developing FTJ-based nanoscale transducers, ultrahigh-density nonvolatile random-access memories and other novel functional devices.

In order to enrich the properties of ferroelectric materials and to extend their application scope, obtaining tunable physical effects and their coupling in ferroelectric materials has been a notable research trend in recent years. It is known that the properties of ferroelectric material can be tuned by electrical/magnetical field, thermal exchange, mechanical loads and stoichiometric composition. Among the common ferroelectrics, ferroelectric perovskite-type oxides with the general formula of ABO$_3$ are particularly sensitive to their elemental composition and stoichiometric ratio. Specially, it is known that most of the metal elements in the Periodic Table are stable in a perovskite-type oxide

---

[a] Corresponding author, Electronic address: zhengy35@mail.sysu.edu.cn,
[b] Electronic address: wangbiao@mail.sysu.edu.cn

structure, and multicomponent perovskites can also be synthesized in experiment, which gives rise to substituted perovskites with formula of $A_\delta A'_{1-\delta} B_\gamma B'_{1-\gamma} O_3$. Moreover, slightly non-stoichiometric perovskites, i.e., with slight deficiency or excess of A, B or O, can also exist and show modified properties from those of the stoichiometric ones. As a result, perovskites exhibit a very broad diversity of properties. For example, a conexistence of conductivity and ferroelectricity has been recently obtained in doped $BaTiO_3$ material. It is known that $BaTiO_3$ material will undergo an insulator-metal transition if the oxygen vacancy concentration reaches a certain value.[6] Such oxygen-deficient $BaTiO_3$ already has some applications like thermistors[7,8] and photoactive capacitors.[9,10] Normally, it is commonly believed that metallic material can not possess ferroelectricity as the itinerant electrons can screen the long-range Coulomb interaction and destroy the ferroelectric distortion. Recently, Kolodiazhnyi *et al.* have found that $BaTiO_3$ heavily-doped with oxygen vacancies can exhibit both conductivity and ferroelectricity.[11] They thus suggest that the doping-induced itinerant electrons not only give rise to insulator-metal phase transition, but also stabilize the ferroelectric distortion in $BaTiO_3$ with oxygen vacancies.

On the other hand, it appears that the oxygen deficiency can change the normally-insulating $BaTiO_3$ into semiconducting or conducting while maintains its ferroelectricity. Oxygen vacancy is a donor dopant, and it is known that the substitution of specific metal elements is another important kind of donor dopant in $BaTiO_3$. A question naturally arises: does the donor-type substitution acts in the same way as oxygen deficiency? If it does, we suggest that donor-type substitution can also be ultilized to improve the conductivity of ferroelectric $BaTiO_3$. While if it does not, then the results in Ref. 11 may be attributed to lattice relaxation mediated by atomic vacant positions[12] rather than itinerant electrons induced by oxygen deficiency. Therefore, studying the donor-type substitutional doped $BaTiO_3$ is helpful to understand the nature of the coexistence of ferroelectricity and conductivity.

According to the above, we are going to carry out theoretical simulation on the doped $BaTiO_3$ in the present work. The simulation is performed in a $Pt/BaTiO_3/Pt$ two probe system, i.e., a ferroelectric tunnel juntion structure using Pt as electrodes and $BaTiO_3$ thin film as the tunneling barrier. At present, we will focus on the donor doping in order to compare our results with Ref. 11. Generally speaking, there are two kinds of typical donor-type substitutional doping in $BaTiO_3$, i.e., Ba being replaced by a trivalent ion such as La, or Ti being replaced by a pentavalent ion such as Nb. The difference in ionic radius of Ti and Nb is much smaller than the difference between Ba and La, which means that the Nb_{Ti} substitution is more likely to maintain the original ferroelectric properties of $BaTiO_3$. Therefore, we will specifically study the Nb_{Ti} substitution in $BaTiO_3$-based FTJs. In theoretical simulation, the Nb_{Ti} substitution can be placed at any Ti position in the barrier, and the effect is expected to be different. On the other hand, the number and distribution of Nb_{Ti} substitution will also affect the result. Among all possible doping cases, Nb_{Ti} substitution placed at the interface layer is especially noteworthy. As the original Pt/TiO_2 interface is replaced by Pt/NbO_2 interface at the Nb_{Ti} substitution position, new interface effects will arise. For example, the band offset at the interface will change, and affect the charge transfer between the barrier and the electrode. Moreover, new chemical bonds may form at the Pt/NbO_2 interface, which has significant effects on the interface dipole of the barrier. As a result, Nb_{Ti} substitutions near the interface should bring more fruitful controllability of properties. In this paper we will focus on the influence of interfacial Nb_{Ti} substitution on the structural and electronic properties of $BaTiO_3$-based FTJs.

II. MODELS AND METHODS

The atomic structure of the simulated FTJs are schematically shown in Fig. 1. We consider FTJ configurations with the lowest interface energy,[13] i.e., with Pt atoms situated above the oxygen atoms on the TiO_2 terminated surface in the following calculations. The interface distances for perfect $BaTiO_3$ and Nb-substitution $BaTiO_3$ are optimized to minimize the total energy of the system in every case. The FTJs are under short-circuit boundary condition, and the Nb_{Ti} substitution is placed at the interfacial TiO_2 layer to simulate the interface effect. The thickness of the Platinum electrode slab is 15 atom layers, which is sufficient to converge the interface states. The simulated FTJs can be divided into two types: symmetric structures, i.e., $Pt/(TiO_2\text{-}BaO)_m\text{-}TiO_2/Pt$ (labeled as BTO-SYM,

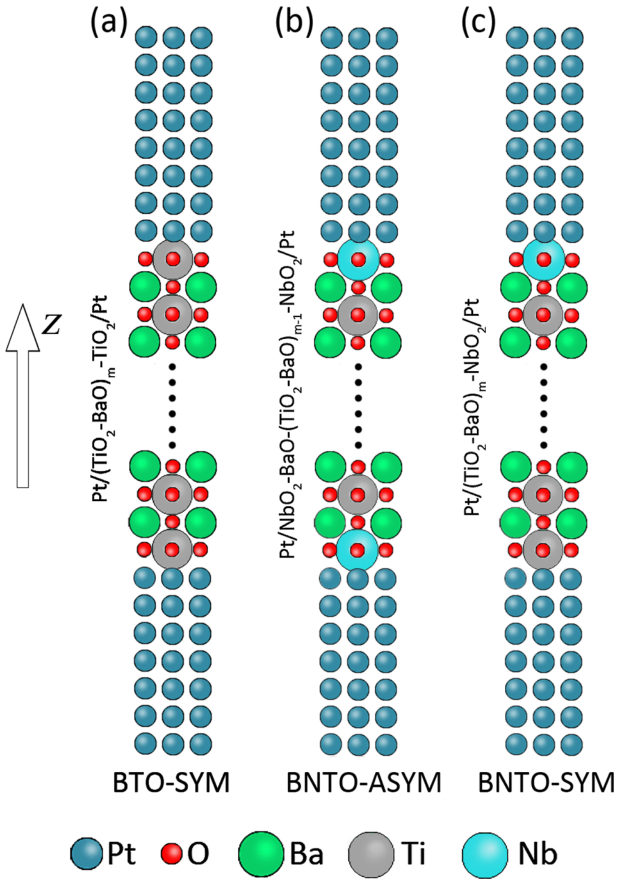

FIG. 1. Schematic side view of the layer-by-layer atomic positions of the simulated FTJs. From left to right is Pt/(TiO_2-BaO)$_m$-TiO_2/Pt, Pt/NbO_2-BaO-(TiO_2-BaO)$_{m-1}$-NbO_2/Pt, and Pt/(TiO_2-BaO)$_m$-NbO_2/Pt tunnel junction.

see Fig. 1(a)) and Pt/NbO_2-BaO-(TiO_2-BaO)$_{m-1}$-NbO_2/Pt (labeled as BNTO-SYM, see Fig. 1(b)), and asymmetric structure Pt/(TiO_2-BaO)$_m$-NbO_2/Pt (labeled as BNTO-ASYM, see Fig. 1(c)). In these FTJs, there are various properties which can be tuned by the barrier thickness. For example, the spontaneous polarization in doped FTJ might have critical thickness, and the conductance of the FTJ certainly depends on the thickness. Such size effects can be revealed by calculating different FTF thicknesses. To study size effects, we simulate three different barrier thickness (the number of perovskite unit-cells m takes the value of 2, 3 and 4) for each type of FTJ structure. Futhermore, in the asymmetric Pt/(TiO_2-BaO)$_m$-NbO_2/Pt FTJs, the polarization can point to either Pt/TiO_2 or Pt/NbO_2 interface. To be clear, we denote symbols "$P \rightarrow$" and "$P \leftarrow$" to represent the former and the latter one respectively. Therefore, via simulating all possible different FTJ configurations, we are able to systematically investigate the size effect and interface effect of interfacial Nb-doped Pt/$BaTiO_3$/Pt FTJ. We calculate the local polarization of FTJ barrier by evaluating $P = \sum Z_i^* U_i$,[14] where Z_i^* is the Born effective charge of the ith ion and U_i is the displacement of the ith ion from its position in the centrosymmetric configuration. We use the density functional perturbation theory (DFPT) method as implemented in VASP to obtain the Born effective charge tensors of the barrier ions in FTJ.[15] Currently the DFPT method in VASP is not implemented for metallic material. Considering that the Fermi-level of barrier may become occupied by electron states due to the interaction with metallic electrodes, We calculate the Born effective charges in a 3×3×3 $BaTiO_3$ supercell with the central $BaTiO_3$ unit cell replaced by $BaNbO_3$ unit cell. The in-plane lattice constant a and b of the supercell are constrained to 11.6004 Å and lattice constant c is freely relaxed.

Another fact worth noting is that the $\mathrm{Nb_{Ti}}$ substitution in $\mathrm{BaTiO_3}$ may possess a variety of charge states. Using Kröger–Vink notation,[16] a charge-neutral oxygen vacancy in $\mathrm{BaTiO_3}$ can be expressed as $\mathrm{V_O^{\times}}$. In this case, the non-bonding d-orbital electrons in Ba/Ti ions adjacent to the O vacancy positions become itinerant electrons. Similarly, a neutral substitutional Nb atom positioned on the orginal Ti atom position ($\mathrm{Nb_{Ti}^{\times}}$) in $\mathrm{BaTiO_3}$ can provide a d-orbital non-bonding electron as itinarant electron. A charged $\mathrm{Nb_{Ti}^{\bullet}}$ substitution is a different situation. As the system will always remain charge neutral in experiment, $\mathrm{Nb_{Ti}^{\bullet}}$ substitution will still generate an itinerant electron, but the defect level of $\mathrm{Nb_{Ti}^{\bullet}}$ is not equal to $\mathrm{Nb_{Ti}^{\times}}$, thus their contribution to conductivity are different. Since we are going to compare our results with the oxygen deficiency results, thus the $\mathrm{Nb_{Ti}}$ substitution we are going to simulate in the following is charge neutral (i.e. $\mathrm{Nb_{Ti}^{\times}}$). We calculated the formation energy of $\mathrm{Nb_{Ti}^{\bullet}}$ and $\mathrm{Nb_{Ti}^{\times}}$ substitution in bulk $\mathrm{BaTiO_3}$[17] and found that the $\mathrm{Nb_{Ti}^{\times}}$ point defect is more stable than $\mathrm{Nb_{Ti}^{\bullet}}$ under certain condition, which indicates that the $\mathrm{Nb_{Ti}^{\times}}$ substitution can be obtained in experiment.

We perform density functional theory (DFT) calculations within local density approximation (LDA)[18] and use projector augmented wave (PAW)[19] method as implemented in the Vienna *Ab-initio* Simulalation Package (VASP).[20,21] An energy cutoff of 500 eV is used for a plane wave basis, with a $6 \times 6 \times 1$ Monkhorst–Pack grid for k-point sampling for FTJ structures.[22] Following Ref. 23, we constrain the in-plane lattice constant of the FTJ structures to the theoretical equilibrium value of cubic $\mathrm{SrTiO_3}$ (3.8668 Å). As a result, the $\mathrm{BaTiO_3}$ FTF is compressed in the x-y plane and the polarization along z-axis is stabilized. All the FTJ structures are fully relaxed until the atomic force components are smaller than 0.01 eV/Å and the stress component along the z-direction is smaller than 0.1 GPa.

To investigate the electronic transport properties of the Nb-doped Pt/$\mathrm{BaTiO_3}$/Pt FTJs, we employ the Atomistic Toolkit simulation package (ATK)[24,25] which combines non-equilibrium Green's function method with DFT calculations.[26] Exchange correlation potentials with Perdew-Zunger parameterization of the localized density approximation (LDA.PZ)[27] are used. To ensure accuracy, the plane-wave basis set is chosen to be double zeta polarized. The Brillouin zone of the system is sampled by a $10 \times 10 \times 100$ k-point mesh for the self-consistent calculations and 50×50 k-point mesh for the transport coefficient spectra and conductance calculations. The electron temperature in the electrodes is set to 1200 K to ensure convergence.

Based on the optimized structure, the formation energy of point defect is calculated in a supercell generated by a 3×3×3 repetition of the perfect $\mathrm{BaTiO_3}$ unit cell in x, y, and z directions. The substitutional point defects were introduced by removing and adding atoms. the formation energy of $\mathrm{Nb_{Ti}}$ substitution in $\mathrm{BaTiO_3}$ can be expressed as

$$\begin{aligned}\Delta E(\mathrm{Nb},q) &= E_{\mathrm{tot}}(\mathrm{BaNb_{\delta}Ti_{1\text{-}\delta}O_3},q) - E_{\mathrm{tot}}(\mathrm{BaTiO_3},0)\\ &\quad - \mu_{\mathrm{Ti}} + \mu_{\mathrm{Nb}} + q(E_f + E_{\mathrm{VBM}}(\mathrm{BaNb_{\delta}Ti_{1\text{-}\delta}O_3},q)),\end{aligned} \tag{1}$$

where $\Delta E(\mathrm{N}b, q)$ is the formation energy of $\mathrm{Nb_{Ti}}$ substitution with charge state q, $E_{\mathrm{tot}}(\mathrm{BaNb_{\delta}Ti_{1\text{-}\delta}O_3},q)$ is the total energy of the Nb-doped supercell, $E_{\mathrm{tot}}(\mathrm{BaTiO_3},0)$ is the total energy of the perfect supercell, μ_i is the chemical potentials of constituent elemental species i, E_f is the Fermi energy of Nb-doped $\mathrm{BaTiO_3}$, $E_{\mathrm{VBM}}(\mathrm{Nb},q)$ is the valence-band maximum (VBM) of the Nb-doped supercell, which is obtained from

$$\begin{aligned}E_{\mathrm{VBM}}(\mathrm{BaNb_{\delta}Ti_{1\text{-}\delta}O_3},q) &= E_{\mathrm{tot}}(\mathrm{BaTiO_3},0) - E_{\mathrm{tot}}(\mathrm{BaTiO_3},+1)\\ &\quad +\bar{V}(\mathrm{BaNb_{\delta}Ti_{1\text{-}\delta}O_3},q) - \bar{V}(\mathrm{BaTiO_3},0),\end{aligned} \tag{2}$$

where $E_{\mathrm{tot}}(\mathrm{BaTiO_3},0)$ and $E_{\mathrm{tot}}(\mathrm{BaTiO_3},+1)$ are the calculated energies of the perfect supercell with charge state 0 and +1, $\bar{V}(\mathrm{BaNb_{\delta}Ti_{1\text{-}\delta}O_3},q)$ is the calculated macroscopic averaged electrostatic potential of the spatial area far away from the substitutional defect site in the Nb-doped supercell, $\bar{V}(\mathrm{BaTiO_3},0)$ is the averaged electrostatic potential of the perfect supercell. The difference between $E_{\mathrm{tot}}(\mathrm{BaTiO_3},0)$ and $E_{\mathrm{tot}}(\mathrm{BaTiO_3},+1)$ is the VBM of perfect supercell, and the difference between $\bar{V}(\mathrm{BaNb_{\delta}Ti_{1\text{-}\delta}O_3},q)$ and $\bar{V}(\mathrm{BaTiO_3},0)$ is the band alignment value which can line up the band structure of Nb-doped supercell with the perfect supercell.

To determine the chemical potentials of each constituent elemental species, we consider the thermodynamic limits. The chemical potentials of each constituent elemental species are always constrained by the calculated formation enthalpy of $BaTiO_3$ in order to maintain the stability of the host

$$\mu_{\mathrm{Ba}} + \mu_{\mathrm{Ti}} + 3\mu_{\mathrm{O}} = \Delta H_f^{\mathrm{BaTiO_3}} \tag{3}$$

In addition to the host condition, to avoid solid/gas elemental precipitation, the chemical potentials of each constituent elemental species can not be positive, i.e.,

$$\mu_{\mathrm{Ba}} \le 0, \mu_{\mathrm{Ti}} \le 0, \mu_{\mathrm{O}} \le 0, \mu_{\mathrm{Nb}} \le 0 \tag{4}$$

Constraints are also imposed by the calculated formation enthalpies of the competing binary oxides of Ba, Ti and Nb to avoid the formation of alternative phases, i.e.,

$$\mu_{\mathrm{Ba}} + \mu_{\mathrm{O}} \le \Delta H_f^{\mathrm{BaO}}, \tag{5}$$

$$\mu_{\mathrm{Ti}} + \mu_{\mathrm{O}} \le \Delta H_f^{\mathrm{TiO}}, \tag{6}$$

$$\mu_{\mathrm{Ti}} + 2\mu_{\mathrm{O}} \le \Delta H_f^{\mathrm{TiO_2}}, \tag{7}$$

$$2\mu_{\mathrm{Ti}} + 3\mu_{\mathrm{O}} \le \Delta H_f^{\mathrm{Ti_2O_3}}, \tag{8}$$

$$\mu_{\mathrm{Nb}} + \mu_{\mathrm{O}} \le \Delta H_f^{\mathrm{NbO}}, \tag{9}$$

$$\mu_{\mathrm{Nb}} + 2\mu_{\mathrm{O}} \le \Delta H_f^{\mathrm{NbO_2}}, \tag{10}$$

$$2\mu_{\mathrm{Nb}} + 5\mu_{\mathrm{O}} \le \Delta H_f^{\mathrm{Nb_2O_5}}. \tag{11}$$

The phase diagram of the ternary Ba-Ti-O system is shown in Fig. 2,[28] which is derived from the combination of the chemical potentials of Ba, BaO, Ti, TiO,TiO_2, Ti_2O_3 and O_2. The chemical potential of O_2 was calculated from the total energy of the O_2 molecule contained in a cubic

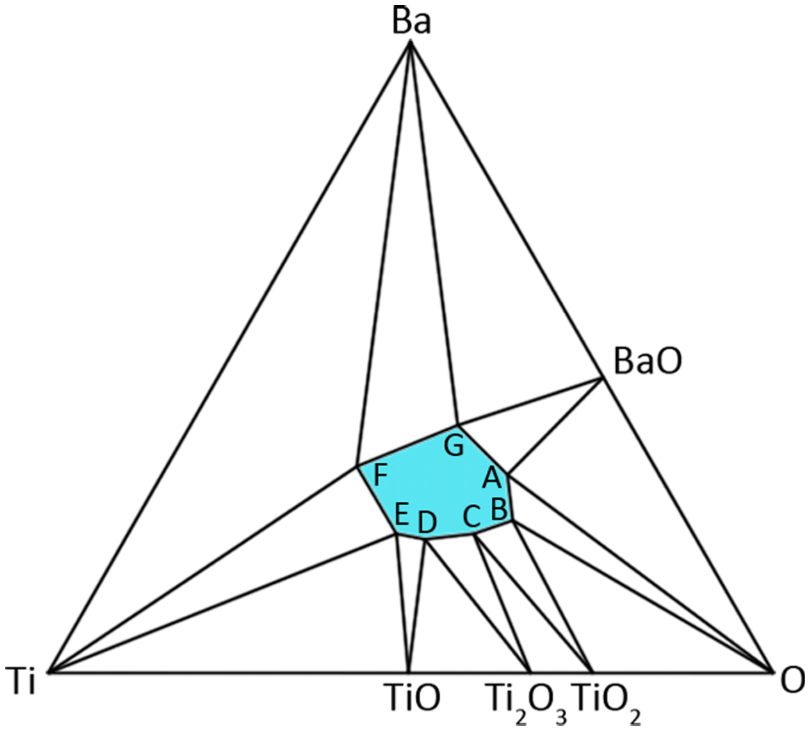

FIG. 2. The schematic phase diagram of the ternary Ba-Ti-O system.

TABLE I. Calculated and experimental formation enthalpies for the $BaTiO_3$ and binary Ba, Nb, and Ti oxides.

Material	Enthalpy of formation (eV/atom)	
	Calculation	Experimental
$BaTiO_3$	-3.706	-4.168[a]
BaO	-3.030	-2.873[b]
TiO	-2.625	-2.816[c]
TiO_2	-3.620	-3.270[d]
Ti_2O_3	-3.116	-3.078[e]
NbO	-2.350	-2.212[f]
NbO_2	-2.957	-2.885[g]
Nb_2O_5	-3.274	-2.932[h]

[a] Reference 29.
[b] Reference 30.
[c] Reference 31.
[d] Reference 32.
[e] Reference 33.
[f] Reference 34.
[g] Reference 35.
[h] Reference 35.

vacuum box with length of 10 angstroms. The vertices of the triangle correspond to three dominant component chemical potentials and the compounds are placed on the edge according to their stoichiometric proportion. Points A–G denoted the seven possible chemical-potential combinations and the region enclosed by these seven points define the thermodynamically equilibrium region of the ternary system under different chemical potentials. At points A and B, the chemical potentials for O are similar to a strong oxidation condition like those $BaTiO_3$ sample grown in an O_2 rich environment. On the contrary, at point G the system is in a strong reduction condition.

III. RESULTS AND DISCUSSION

A. Phase stability of Nb_{Ti} substitution in $BaTiO_3$

The calculated formation enthalpies of competing binary oxides in the synthesizing of $BaNb_{\delta}Ti_{1-\delta}O_3$ are listed in Table I. According to Eqs. (5) to (11), these results are essential to determine the chemical potentials of Ti and Nb elements at each chemical potential equilibrium point in Fig. 2. The experimental enthalpies of formation are also given in Table I. It can be seen that the calculated enthalpies of formation are in general agreement with the experimental values.[29–35]

After the calculation of chemical potentials of Ti and Nb, the formation energies of various Nb_{Ti} substitutions in $BaTiO_3$ with different charge states can be calculated from Eqs. (1) and (2). Here we consider the two most typical charge states of Nb/quadrivalent-metal substitution, i.e., charge neutral and +1 charged. The calculated formation energies of $Nb_{Ti}^{\times}$ and $Nb_{Ti}^{\bullet}$ as a function of the elemental and electronic chemical potentials are shown in Fig. 3. The formation energy of charged and charge neutral doping is only shown when it has the lower energy. The slope of a line corresponds to a charge defect state and the inflection point indicates a transition between charged and charge neutral states. It is shown that the $Nb_{Ti}^{\bullet}$ is the dominant defect above the top of valence band, but its energy increase as the Fermi level increase. At the bottom of the conduction band, the $Nb_{Ti}^{\times}$ become stable. As can be seen from Fig. 3, at point C under oxidization condition, the formation energies for both $Nb_{Ti}^{\bullet}$ and $Nb_{Ti}^{\times}$ are minimized. This is because TiO_2 and Ti_2O_3 are strong competitive reaction products which would easily cause Ti deficiency, thus the Nb_{Ti} sustitution is more likely to form.

B. Ferroelectric polarization

To explore the ferroelectric stability of Nb-doped FTJs, we relax the FTJ configurations in Fig. 1. For BNTO-ASYM FTJs, the ferroelectric distortions from Pt/TiO_2 to Pt/NbO_2 interface

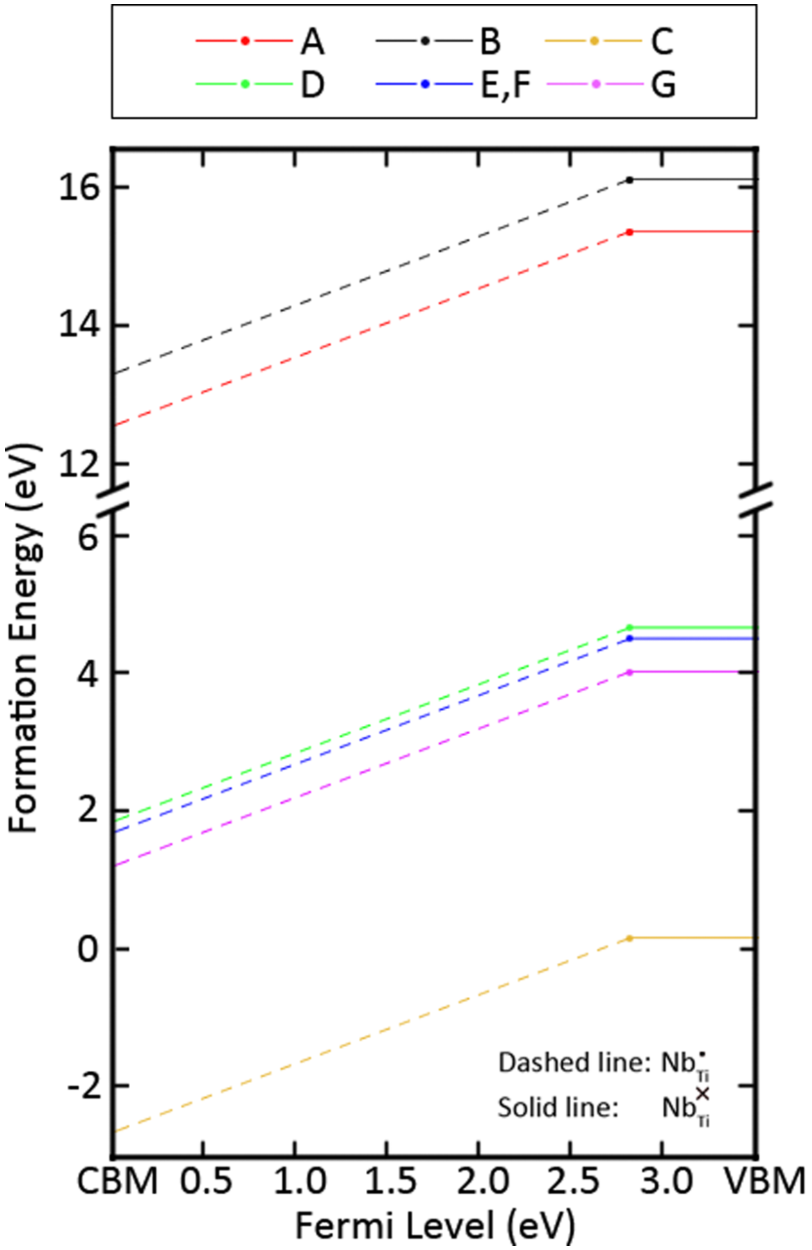

FIG. 3. Formation energies of Nb_{Ti} substitution in cubic $BaTiO_3$ as a function of the Fermi level at chemical potential equilibrium points. The range of energy is set to the experimental bandgap width of perfect Barium titanate.

and from Pt/NbO_2 to Pt/TiO_2 interface are initially imposed, and we found that the polarization of the relaxed structure always point to Pt/NbO_2 interface when $m \leq 3$. When m=4, a ferroelectric polarization points to Pt/TiO_2 interface can be obtained after relaxation. Further analysis indicates that there is a large dipole points to the adjacent Pt electrode at the interfacial NbO_2 layer. If the thickness of the tunnel junction barrier is smaller than 4 unit-cells, this interface dipole seems can determine the polarization direction of the entire junction. When the thickness of barrier increases, the properties of barrier becomes closer to bulk material, thus the polarization becomes switchable regardless of the existence of anomalous interface dipole. As a result, an overall polarization points to Pt/TiO_2 interface in BNTO-ASYM FTJ can stably exists when $m \geq 4$. In the following, we simulate ten different FTJs, i.e., three BTO-SYM configurations (m=2,3,4), three

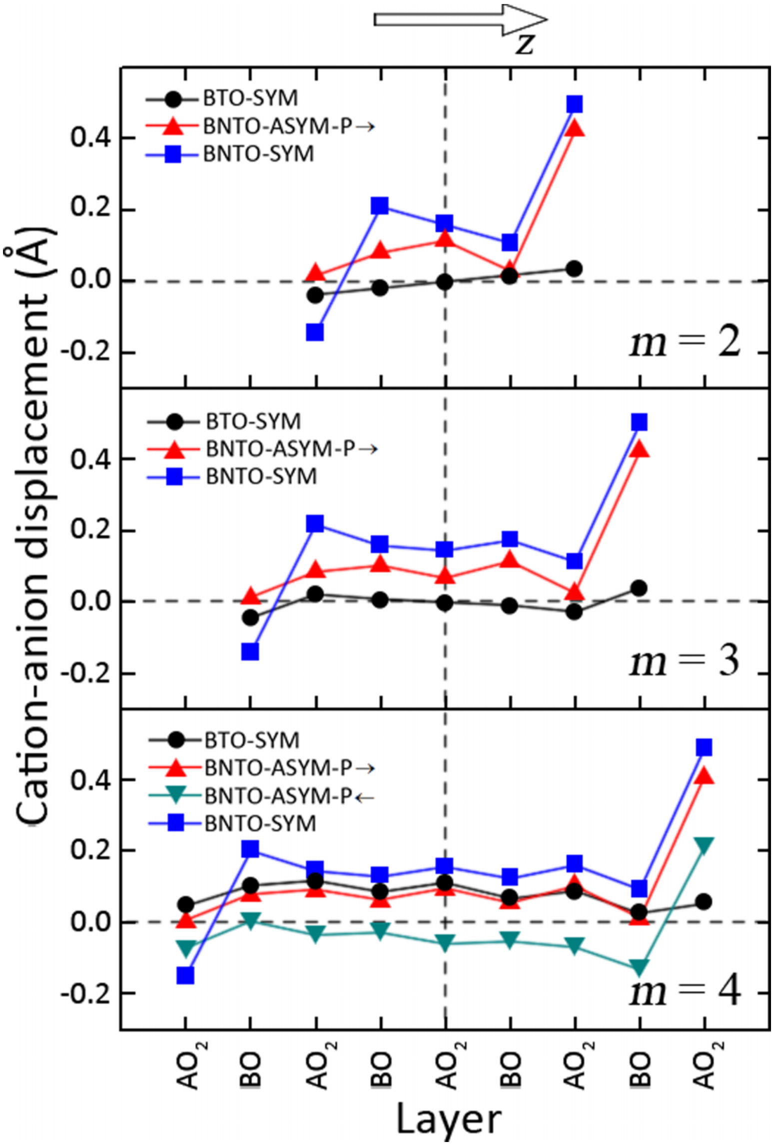

FIG. 4. The layer rumpligs along the z-direction within the fully relaxed FTJ configurations. The distribution of Ti-O/Nb-O rumpling of [001] TiO_2/NbO_2 monolayers and Ba-O rumpling of [001] BaO monolayers of the relaxed FTJs are dipicted.

BNTO-SYM configurations (m=2,3,4), three BNTO-ASYM-P → configurations (m=2,3,4), and one BNTO-ASYM-P ← configuration (m=4).

Fig. 4 shows the layer rumplings (i.e. the relative anion-cation displacements) of simulated FTJs in the z-direction. A positive layer rumpling indicates a positive z-directed local electric dipole moment. Centrosymmetric $BaTiO_3$ is a configuration in which the sums of both TiO_2 and BaO layer rumplings are zero, and the out-of-plane net polarization is also zero. For BTO-SYM tunnel junctions, it can be seen that when the number of unit-cells (m) of the barrier is above three, the Ti-O and Ba-O rumpling distribution is positive, indicating the occurance of net polarization across the barrier and a polarization-related asymmetric field. Otherwise, if $m \leq 3$, the Ti-O rumpling distribution becomes centrosymmetric, which indicats a zero net polarization. Similar trend is found in the Ba-O rumplings. Therefore, the ferroelectric critical thickness of this type of tunnel junctions is four unit-cells. Previous works have found that the ferrelectric critical thickness in $BaTiO_3$-based FTJ under the short-circuit boundary condition is larger than 1.2 nm,[36–38] which is consistent with our result.

However, in the Nb-doped FTJs, the ferroelectric critical thickness dramatically vanished. The calculated results of BNTO-ASYM tunnel junctions are depicted in Fig. 4. We found that the net layer rumpligs remain non-zero for all thickness and increases with the decrease of the thickness of the barrier, indicating an abnormal enhancement of ferroelectricity. Remarkable Nb-O rumpling over 0.4Å (points to the adjacent Pt electrode) is found at the Pt/NbO_2 interface. However, the calculated results of BNTO-SYM tunnel junctions are further different from BNTO-ASYM tunnel junctions. In BNTO-ASYM tunnel junctions, the dipole of the interfacial NbO_2 layer is fixed and always points to the electrode. This phenomenon is also found in the BNTO-SYM FTJs, but the anion-cation displacements of the two interfacial NbO_2 layers are different. For all simulated BNTO-SYM FTJs, a smaller Nb-O displacement over 0.15Å is found at one interfacial NbO_2 layer and a larger Nb-O displacement over 0.4Å is found at the other one. At the same time, the overall ferroelectric distortion of the barrier always points to the Pt/NbO_2 interface with larger Nb-O displacement. Thus one of the Pt/NbO_2 interface enhance the overall polarization while the other one weaken it. However, as the Nb-O displacement along the polarization direction is larger than the one against it, the collective effect of Pt/NbO_2 interface is to enhance the overall polarization. From Fig. 4, it is clear to see that even the BNTO-SYM and BNTO-ASYM FTJs with $m = 2$ can possess stable ferroelectric distortion, which is almost the lowest scale of ferroelectricity. Another noteworthy phenomenon is that, in the BTO-SYM FTJ, the layer rumplings at the central region of FTF barrier are close to bulk value but decrease near the interface. This result is compatible with the observed interface-induced suppression of polarization in experiments. However, in the interfacial Nb-doped FTJ, the layer rumplings at the Nb-doped interface layers are significantly larger than the central region, which is the typical characteristic of metal-oxide interfacial ferroelectricity.[39]

The calculated spontaneous polarization in different FTJs are shown in Fig. 5(a). To study the change of free energy with the orientation of the interfacial Nb_{Ti} substitution induced polarity, the calculated DFT free energy results are shown in Fig. 5(b). It can be seen that the Nb_{Ti} substitution not only enhances the polarization, but also reduces the total energy, which indicates that the fixed Nb induced polarization is stable. we further calculate the longitudinal force constant k^L of Ti and Nb ions in a stable Pt/TiO_2 and Pt/NbO_2 interface, and found that k^L_{Ti} = -0.13 a.u., and k^L_{Nb} = -0.22 a.u., which indicates the existence of strong fixed electronic dipole at the Pt/NbO_2 interface. This interface dipole would break the centrosymmetric stability of FTF barrier, thus results in the disappearance of ferroelectric critical thickness.

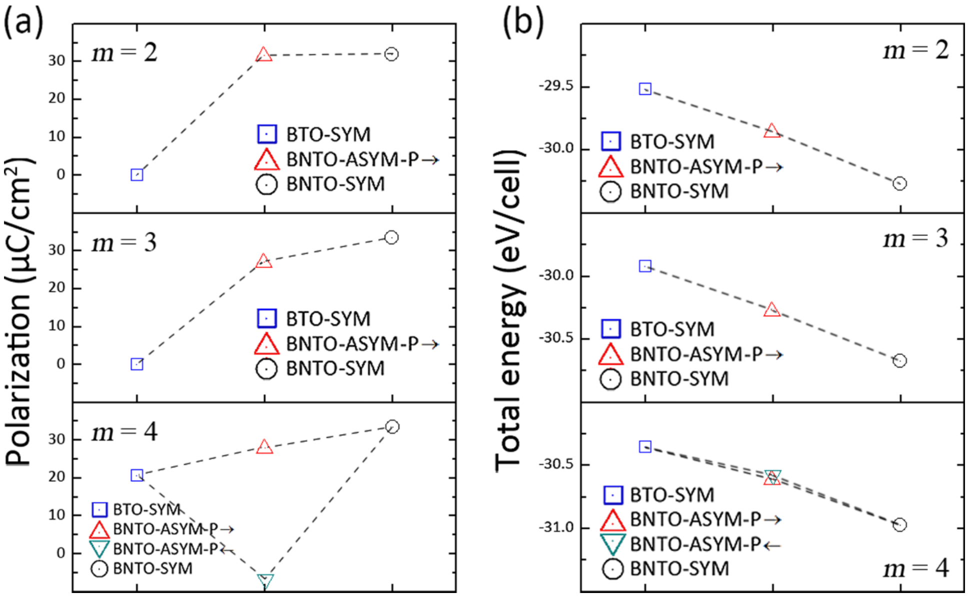

FIG. 5. (a) The calculated polarization in each simulated FTJ. (b) The calculated total energy per unit cell in each simulated FTJ.

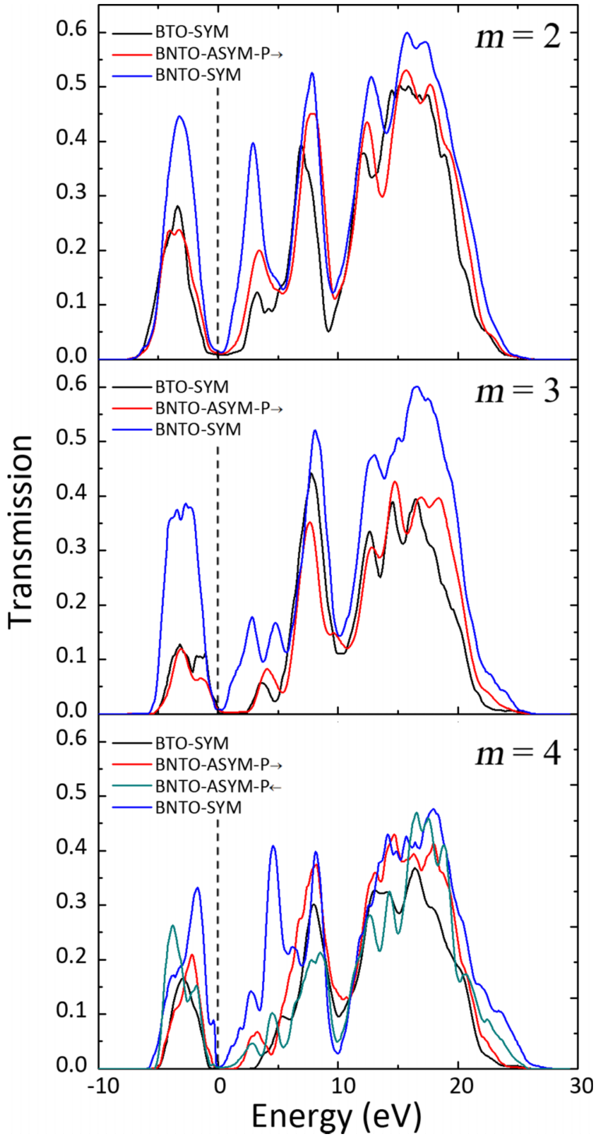

FIG. 6. Dependence of the transmission spectra on the energy for different FTJs. The Fermi level is set to zero.

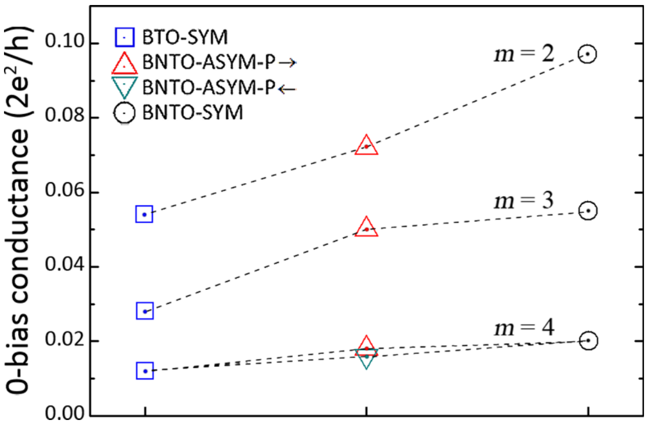

FIG. 7. The calculated zero-bias conductance of different FTJs.

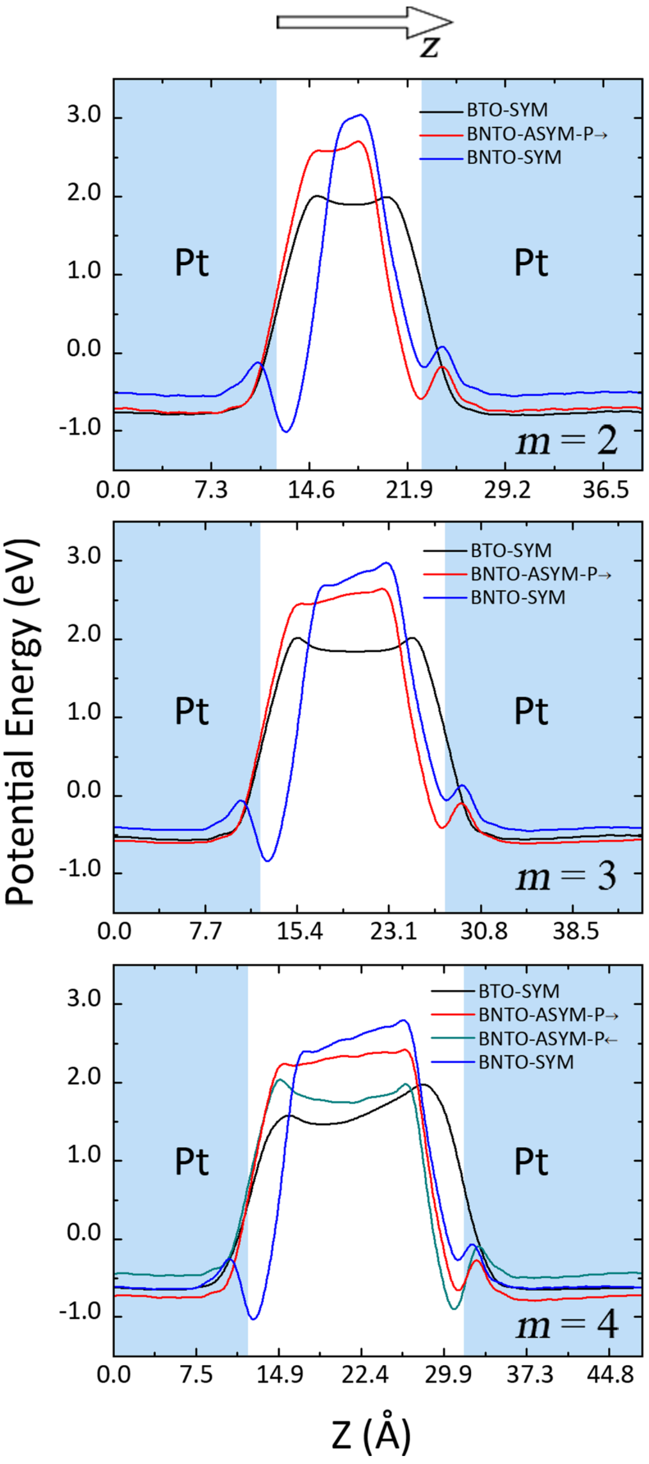

FIG. 8. The macroscopic averaged electrostatic potential along the z-direction of each FTJ.

C. Electronic properties

As previously mentioned, $\mathrm{Nb}_{\mathrm{Ti}}^{\times}$ substitution might induce similar carrier doping effect as oxygen deficiency, which can improve the electronic conductivity of $BaTiO_3$. To investigate this effect, we calculate the transmission spectra of the simulated FTJs. Fig. 6 shows our results. The transmission

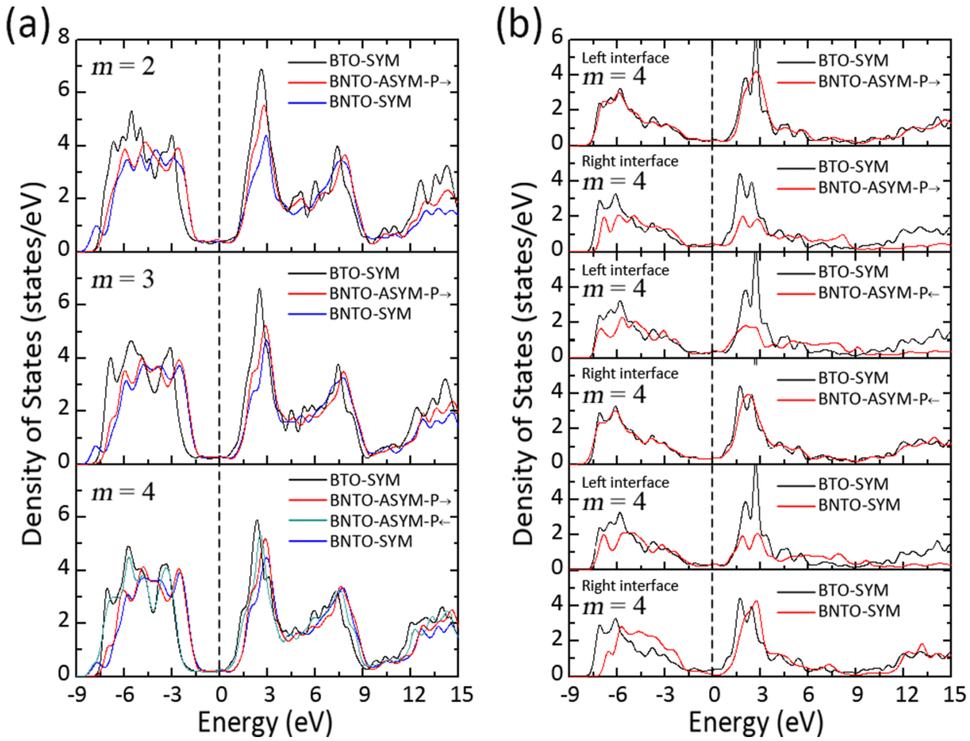

FIG. 9. (a) The calculated local density of the states (LDOS) of the junctions in simulated FTJs. (b) The LDOS of the interfacial TiO_2/NbO_2 atomic layers of doped FTJs with m=4. The polarization direction is from left interface to right interface. The Fermi level is set to zero.

valley near the Fermi level coincides with the band gap in the LDOS of ferroelectric thin film barrier. The general trend is that with the increase of the Nb_{Ti} substitution concentration, the total transmission coefficients integrated with overall energy significantly increases, which indicates that the interfacial Nb_{Ti} substitution opened new transmission channels in the FTJ.

Another noteworthy phenomenon is that the Nb_{Ti} substitution significantly increases the transmission coefficients far from the Fermi energy, while this effect is less obvious near the Fermi level. The transmission coefficients near the Fermi level describe the conductivity of FTJ under small bias, and the value at the Fermi level corresponds to the FTJ conductivity under zero-bias and absolute zero temperature. To investigate the low-bias electrical conductivity, we further calculate the zero-bias conductivity of each FTJ. The results of conductivity are shown in Fig. 7. It is clear that the substitution effectively improves the electrical conductivity of FTJ at zero bias. In general, the paraelectric-phase conductance of ferroelectric tunnel junction is higher than ferroelectric-phase, since the ferroelectric polarization increases the width of band gap. However, in Nb-doped FTJs, the enhanced polarization and conductivity can exist simultaneously. This result is very similar to Ref. 11.

To explore the mechanism of conductivity enhancement induced by Nb_{Ti} substitution, we calculated the macroscopic averaged electrostatic potential profile[40–43] of the ground state electron gas in each simulated FTJ. The results are shown in Fig. 8. It can be seen that in Nb-doped FTJs, the electrostatic potential near the Pt/NbO_2 interface drastically drops. As a result, the effective width of the tunnel barrier decreases. Another interesting result is that in the $Pt/(TiO_2\text{-}BaO)_4\text{-}NbO_2/Pt$ FTJ, a great change takes place in the average height of electrostatic potential barrier when the polarization is flipped (from $P \rightarrow$ to $P \leftarrow$). This phenomenon indicates that the polarization reversal is accompanied by giant tunnelling elctroresistance effect. However, in thinner asymmetrical doped Nb-doped FTJs, as the spontaneous polarizations have only one stable direction, external bias is needed to flip the polarization and generate the giant tunnelling elctroresistance effect.

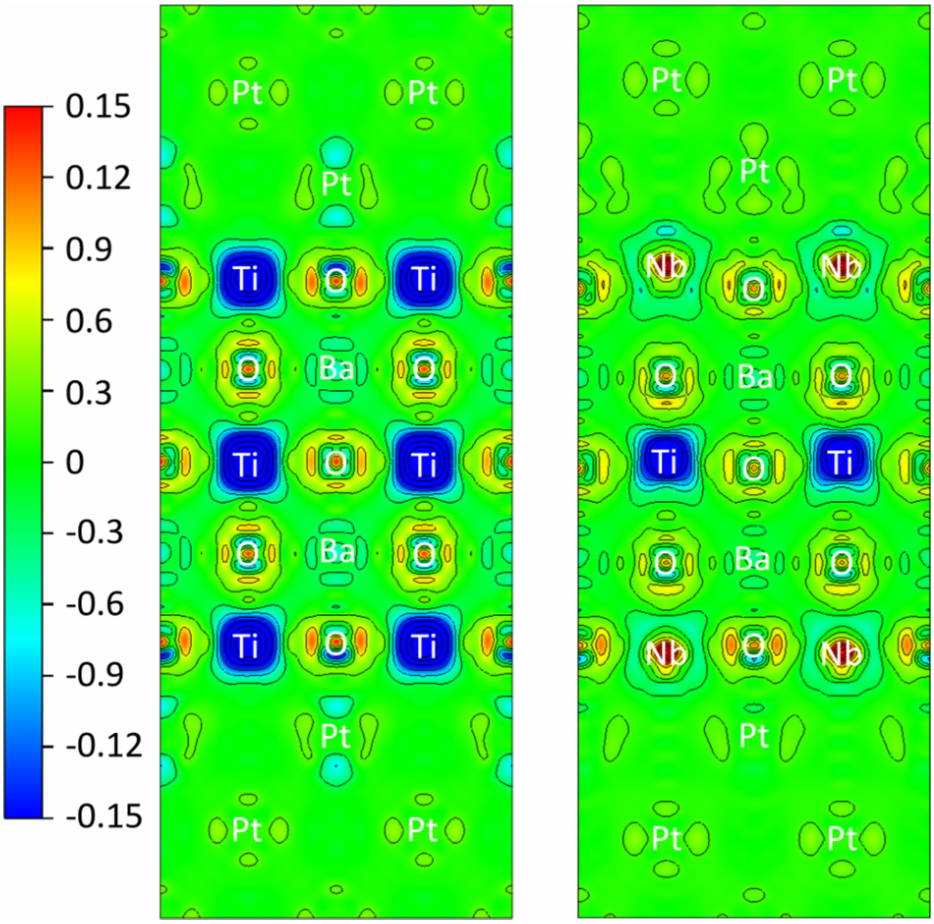

FIG. 10. The contour plot on the (200) crystallographic plane of the differential charge density profiles of BTO-SYM and BNTO-SYM FTJs with m=2.

To gain insight into the influence of the interfacial Nb_{Ti} substitution on the electronic structure of the $BaTiO_3$ tunnel junction, we calculate the local density of states (LDOS) of the FTJs as shown in Fig. 9(a). The Fermi level is set to zero and depicted by the dot line. Results indicate that the valence band of the barrier tends to shift towards a higher level of energy when the number of Nb_{Ti} substitution increases. The conduction band also tends to shift, but the shifting offset is significantly smaller than valence band. As a result, the bandgap is shortened, which explains the increase of transmission coefficient at Fermi level. To further study the interface effect, the calculated LDOS of the interfacial TiO_2/NbO_2 layers in BTO-SYM, BNTO-SYM and BNTO-ASYM FTJs with barrier thickness m = 4 are depicted in Fig. 9(b). The shifting of valence band can also be observed at an interfacial NbO_2 layer. At the same time, some new hybrid peaks appear in the conduction band due to the hybridization between the polarized NbO_2 interface layer and the adjacent Pt electrode.

We further plot the 2D section on the (200) crystallographic plane and the macroscopic average of the differential charge density profiles of BTO-SYM and BNTO-SYM FTJs. Differential charge density is defined as the difference between self-consistent charge density and the non-self-consistent charge density (i.e., the superposition of atomic charge densities), so it can reflect the gain and loss of charges before and after the self-consistent calculation. The results are shown in Fig. 10. It can be seen in the perfect tunnel junctions, Ti ions in the interface layers lose charges after the self-consistent calculation, on the contrary, Nb ions in the NbO_2 interface layers gain charges after the self-consistent calculation. This result indicates the forming of interfacial electron accumulation layer (also known as anti-barrier) when the interface TiO_2 layers are doped with Nb_{Ti} substitution, it also explains the electrostatic potential drop at the interface. From

Fig. 8, Fig. 9 and Fig. 10, conclusions can be drawn that the interfacial electron accumulation layers decreases the barrier width and increases the carrier concentration in the FTF barrier, thus it can enhance the conductivity of FTJ. On the other hand, the eletron gas at the heterointerface would possess mobility as the temperature and external bias increased,[44] thus its impact on the conductivity of FTJ may be more significant in the conditions of high temperature and large external bias.

IV. CONCLUSION

In summary, the equilibrium ionic configurations, ferroelectric distortions and electronic properties of Pt/$BaNb_{\delta}Ti_{1-\delta}O_3$/Pt FTJ with interfacial layers doped by Nb is investigated using density functional calculations combined with the non-equilibrium Green's function method. Compare to the perfect Pt/$BaTiO_3$/Pt FTJ, the interfacial Nb-substitution reduce the ferroelectric critical thickness of ferroelectric thin film barrier to below two unit-cells, which can be regarded as the vanishing of critical thickness from a practical point of view. Surprisingly, the spontaneous polarization in the Nb-doped ferroelectric thin film barrier is larger than in perfect ferroelectric thin film barrier, which is resulted from the ferroelectricity enhancement effect in the Pt/NbO_2 interface. On the other hand, the negative carrier doping and anti-barrier at the interface induced by Nb_{Ti} substitutional doping also enhance the conductivity of FTJ. This indicates the coexistence of ferroelectricity and enhanced conductivity in FTJ configuration, which could have significant impact on the functional design of FTJ-based devices. We are looking forward to further theoretical and experimental works to confirm these findings.

ACKNOWLEDGEMENTS

The authors acknowledge the financial support of the National Natural Science Foundation of China (NSFC) (Nos. 51172291, 11232015, 11372361, 11474363). Yue Zheng also thanks support by the Fundamental Research Funds for the Central Universities, New Century Excellent Talents in University, Research Fund for the Doctoral Program of Higher Education, Fok Ying Tung Foundation, Guangdong Natural Science Funds for Distinguished Young Scholar.

[1] M. Y. Zhuravlev, R. F. Sabirianov, S. S. Jaswal, and E. Y. Tsymbal, Phys. Rev. Lett. **4**, 246802 (2005).
[2] E. Y. Tsymbal and H. Kohlstedt, Science **313**, 181 (2006).
[3] A. Gruverman, D. Wu, H. Lu, Y. Wang, H. W. Jang, C. M. Folkman, M. Y. Zhuravlev, D. Felker, M. Rzchowski, C. B. Eom, and E. Y. Tsymbal, Nano. Lett. **9**, 3539 (2009).
[4] Y. Zheng and C. H. Woo, Nanotechnology **20**, 075401 (2009).
[5] V. Garcia, S. Fusil, K. Bouzehouane, S. E. Vedrenne, N. D. Mathur, A. Barthelemy, and M. Bibes, Nature **460**, 81 (2009).
[6] T. Kolodiazhnyi, Phys. Rev. B. **78**, 045107 (2008).
[7] G. H. Jonker, Solid-State Electron. **7**, 895 (1964).
[8] A. Al-Shahrani and S. Abboudy, J. Phys. Chem. Solids. **61**, 966 (2000).
[9] Y. A. Park, K. D. Sung, C. J. Won, J. H. Jung, and N. Hur, J. Appl. Phys. **114**, 094101 (2013).
[10] J. Hwang, T. Kolodiazhnyi, J. Yang, and M. Couillard, Phys. Rev. B. **82**, 214109 (2010).
[11] T. Kolodiazhnyi, M. Tachibana, H. Kawaji, J. Hwang, and E. Takayama-Muromachi, Phys, Rev. Lett. **104**, 147602 (2010).
[12] A. V. Kimmel, P. M. Weaver, M. G. Cain, and P. V. Sushko, Phys, Rev. Lett. **109**, 117601 (2012).
[13] N. Sai, A. M. Kolpak, and A. M. Rappe, Phys. Rev. B. **72**, 020101(R) (2005).
[14] W. J. Chen, Yue Zheng, X. Luo, B. Wang, and C. H. Woo, J. Appl. Phys. **114**, 064104 (2013).
[15] M. Gajdos, K. Hummer, G. Kresse, J. Furthmüller, and F. Bechstedt, Phys. Rev. B. **73**, 045112 (2006).
[16] F. A. Kröger and H. J. Vink, Solid State Physics **3**, 307 (1956).
[17] X. Luo, B. Wang, and Y. Zheng Y, Phys. Rev. B. **80**, 104115 (2009).
[18] D. M. Ceperley and B. J. Alder, Phys. Rev. Lett. **45**, 566 (1980).
[19] P. E. Blöchl, Phys. Rev. B. **50**, 17953 (1994).
[20] G. Kresse and J. Furthmuller, Phys. Rev. B. **54**, 11169 (1996).
[21] G. Kresse and J. Furthmuller, Comput. Mater. Sci. **6**, 15 (1996).
[22] H. J. Monkhorst and J. D. Pack, Phys. Rev. B. **13**, 5188 (1976).
[23] J. Junquera and P. Ghosez, Nature **422**, 506 (2003).
[24] M. Brandbyge, J. L. Mozos, P. Ordejon, J. Taylor, and K. Stokbro, Phys. Rev. B. **65**, 165401 (2002).
[25] J. M. Soler, E. Artacho, J. D. Gale, A. Garcia, J. Junquera, P. Ordejon, and D. Sanchez-Portal, J. Phys. Condens. Matter **14**, 2745 (2002).
[26] M. C. Payne, M. P. Teter, D. C. Allan, T. A. Arias, and J. D. Joannopoulos, Rev. Mod. Phys. **64**, 1045 (1992).
[27] J. P. Perdew and A. Zunger, Phys. Rev. B. **23**, 5048 (1981).

[28] M. Imaeda, T. Mizoguchi, Y. Sato, H. S. Lee, S. D. Findlay, N. Shibata, T. Yamamoto, and Y. Ikuhara, Phys. Rev. B. **78**, 245320 (2008).
[29] D. R. Lide, *Handbook of Chemistry and Physics*, 85th ed. (CRC Press, Boca Raton, 2004).
[30] G. H. Aylward and T. Findlay, *SI Chemical Data*, 4th ed. (John Wiley & Sons Australia Limited, 1999).
[31] *NIST Chemistry WebBook*, edited by W. G. Mallard and P. J. Linstrom (National Institute of Standards and Technology, Gaithersburg, MD, 2008).
[32] Zumdahl and S. Steven, *Chemical Principles*, 6th ed. (Houghton Mifflin Company, 2010).
[33] G. V. Samsonov, *The Oxide Handbook* (IFI/Plenum, New York, 1982).
[34] H. Inaba, T. Mima, K. Naito, and J. Chem, Thermodynamics **16**, 411 (1984).
[35] M. P. Marozava, L. L. Gestkina, and Z. Obeshei, kximij **29**, 1049 (1959).
[36] J. Junquera and P. Ghosez, Nature **422**, 508 (2003).
[37] G. Gerra, A. K. Tagantsev, N. Setter, and K. Parlinski, Phys. Rev. Lett. **96**, 107603 (2006).
[38] Y. S. Kim, D. H. Kim, J. D. Kim, Y. J. Chang, and T. W. Noh, Appl. Phys. Lett. **86**, 102907 (2005).
[39] M. Stengel, D. Vanderbilt, and N. A. Spaldin, Nature Materials **8**, 392 (2009).
[40] A. Baldereschi, S. Baroni, and R. Resta, Phys. Rev. Lett. **61**, 734 (1988).
[41] M. Peressi, N. Binggeli, and A. Baldereschi, J. Phys. D **31**, 1273 (1998).
[42] Q. K. Li, B. Wang, Y. Zheng, Q. Wang, and H. Wang, Physica Status Solid-Rapid Research Letters **1**, 217 (2007).
[43] M. Q. Cai, Y. Zheng, B. Wang, and G. W. Yang, Appl. Phys. Lett. **95**, 232901 (2009).
[44] A. Ohtomo and H. Y. Hwang, Nature **427**, 423 (2004).